Array-Based Electrical Detection of DNA with Nanoparticle Probes

So-Jung Park, *et al.*

Science **295**, 1503 (2002);
DOI: 10.1126/science.1067003

Science (print ISSN 0036-8075; online ISSN 1095-9203) is published weekly, except the last week in December, by the American Association for the Advancement of Science, 1200 New York Avenue NW, Washington, DC 20005.

3. L. T. Scott, *Pure Appl. Chem.* **68**, 291 (1996) and references cited therein.
4. L. T. Scott, M. S. Bratcher, S. Hagen, *J. Am. Chem. Soc.* **118**, 8743 (1996).
5. R. B. M. Ansems, L. T. Scott, *J. Am. Chem. Soc.* **122**, 2719 (2000).
6. Pyrolyses of **2** were carried out at an oven temperature of 1100°C as described previously for other substrates (*4*, *7*), with a steady stream of nitrogen carrier gas flowing through the sample chamber from a thin capillary connected to a 1-atm reservoir (final pressure with the nitrogen flowing = ~0.01 mm Hg). To promote sublimation of **2**, the sample chamber was heated to 350°C for 45 min and then to 400°C for an additional 60 min. Pyrolysis of a 120-mg sample of **2** at 1100°C, using an unpacked quartz tube, gave 27 mg of crude product in the pyrolysis trap. Filling the pyrolysis tube with quartz rings resulted in a lower material balance and a poorer conversion to C_{60}.
7. A. Necula, L. T. Scott, *J. Anal. Appl. Pyrol.* **54**, 65 (2000).
8. The first 10 reactions summarized in Fig. 2 (steps a through j) were run under essentially standard conditions, and the products were thoroughly characterized by combustion analysis and/or high-resolution mass spectroscopy, ^{1}H nuclear magnetic resonance (NMR), ^{13}C NMR, and, where appropriate, infrared spectroscopy (*9*). The final step (k) was run on a 641-mg scale in 25 ml of *ortho*-dichlorobenzene with 2.4 molar equivalents of $TiCl_4$ at 100°C for 130 min, under conditions similar to those that have proven successful for numerous other aldol trimerizations of related systems in our laboratory (*5*, *9*, *24*). The product (**2**) gave a base peak for the molecular ion in the matrix-assisted laser desorption-ionization (MALDI) mass spectrum (calculated for $C_{60}H_{27}Cl_3$, 852.1178; found, 852.1138), but it is too insoluble to permit complete characterization by ^{1}H NMR spectroscopy. The only significant byproduct in the $TiCl_4$ reaction was the next higher homolog of **2**, the cyclic tetramer (MALDI mass spectrum: calculated for $C_{80}H_{36}Cl_4$, 1136.1571; found, 1136.1540).
9. M. M. Boorum, thesis, Boston College, Chestnut Hill, MA (2001).
10. M. A. Brooks, L. T. Scott, *J. Am. Chem. Soc.* **121**, 5444 (1999).
11. S. Hagen, M. S. Bratcher, M. S. Erickson, G. Zimmermann, L. T. Scott, *Angew. Chem. Int. Ed. Engl.* **36**, 406 (1997).
12. M. Wu, X. Wei, L. Qi, Z. Xu, *Tetrahedron Lett.* **37**, 7409 (1996).
13. For analytical purposes, the product mixtures from the pyrolyses were chromatographed on a Kontron ODS2 Techsphere 5 column (no. 421CTS-155125, with fully end-capped octadecylsilane-covered spherical silica, measuring 125 mm by 4.6 mm, and containing 5-μm particles), monitoring at 335 nm with a diode array UV-VIS detector, and eluting with 55:45 toluene:acetonitrile (0.5 ml/min).
14. For the isolation of C_{60}, a Supelco SUPELCOSIL LC-PAH ODS column (250 mm by 4.6 mm, containing 5-μm particles) was used with UV monitoring at 335 nm and 1:1 toluene:acetonitrile as the eluant (1.2 ml/min). Collection of the effluent from the column commenced ~1 min before the C_{60} peak appeared in the chromatogram and continued for a period of at least 5 min for each run. When a mixture of authentic C_{60} and C_{70} is chromatographed and collected in this manner, both fullerenes are detected in the mass spectroscopic analysis. The product mixture from the pyrolysis, on the other hand, gives only C_{60} and no C_{70}.
15. K. Komatsu, K. Fujiwara, Y. Murata, *Chem. Commun.* **2000**, 1583 (2000).
16. Y. Rubin, M. Kahr, C. B. Knobler, F. Diederich, C. L. Wilkins, *J. Am. Chem. Soc.* **113**, 495 (1991).
17. S. W. McElvany, M. M. Ross, N. S. Goroff, F. Diederich, *Science* **259**, 1594 (1993).
18. Y. Rubin *et al.*, *Angew. Chem. Int. Ed. Engl.* **37**, 1226 (1998).
19. Y. Tobe *et al.*, *J. Am. Chem. Soc.* **120**, 4544 (1998).
20. Y. Tobe *et al.*, *Tetrahedron* **57**, 3629 (2001).
21. L. T. Scott, M. M. Hashemi, D. T. Meyer, H. B. Warren, *J. Am. Chem. Soc.* **113**, 7082 (1991).
22. L. T. Scott *et al.*, *J. Am. Chem. Soc.* **119**, 10963 (1997).
23. L. T. Scott *et al.*, *Pure Appl. Chem.* **71**, 209 (1999) and references cited therein.
24. B. J. McMahon, thesis, Boston College, Chestnut Hill, MA (1997).
25. M. D. Clayton, P. W. Rabideau, *Tetrahedron Lett.* **38**, 741 (1997).
26. N. S. Goroff, *Acc. Chem. Res.* **29**, 77 (1996).
27. Financial support for this work was generously provided by NSF and the U.S. Department of Energy. Fellowships for L.T.S., S.H., and H.W. from the Alexander von Humboldt Foundation, the German Academic Exchange Service, and the Fulbright Foundation, respectively, are also gratefully acknowledged. High-resolution mass spectra were recorded at the University of Illinois, Urbana-Champaign, and the University of California, Riverside.

27 November 2001; accepted 18 January 2002

Array-Based Electrical Detection of DNA with Nanoparticle Probes

So-Jung Park, T. Andrew Taton,* Chad A. Mirkin†

A DNA array detection method is reported in which the binding of oligonucleotides functionalized with gold nanoparticles leads to conductivity changes associated with target-probe binding events. The binding events localize gold nanoparticles in an electrode gap; silver deposition facilitated by these nanoparticles bridges the gap and leads to readily measurable conductivity changes. An unusual salt concentration–dependent hybridization behavior associated with these nanoparticle probes was exploited to achieve selectivity without a thermal-stringency wash. Using this method, we have detected target DNA at concentrations as low as 500 femtomolar with a point mutation selectivity factor of ~ 100,000:1.

A major challenge in the area of DNA detection (*1*) is the development of methods that do not rely on polymerase chain reaction (PCR) or comparable target-amplification systems that require additional instrumentation and reagents that are not ideal for point-of-care or field use. Another restrictive requirement of most DNA detection systems, regardless of their need for PCR, is a thermal-stringency wash to differentiate target strands from ones with mismatches and thus achieve desired analyte selectivity. We previously reported several optical DNA detection methods based on oligonucleotide-modified Au nanoparticles and their size-dependent scattering, catalytic, and absorption properties (*2*–*5*). We also showed that Au particles that are heavily functionalized with oligonucleotides exhibit extraordinarily sharp thermal-denaturation profiles that translate into higher target selectivities (*2*–*5*). We now report a conductivity-based DNA detection method utilizing oligonucleotide-functionalized Au nanoparticles that provides an alternative to existing detection methods (*6*–*11*) and presents a straightforward approach to high-sensitivity and -selectivity, multiplexed detection of DNA.

In the detection scheme (Fig. 1A), selective binding occurs between a shorter "capture" oligonucleotide strand located in the gap between two fixed microelectrodes and a longer "target" oligonucleotide in solution. The target oligonucleotide has contiguous recognition elements that are complementary to the capture strand on one end and on the other to oligonucleotides attached to Au nanoparticles (Fig. 1B). Therefore, when the device with the pair of electrodes is immersed in a solution containing the appropriate probe and target, Au nanoparticle probes fill the gap.

In principle, capacitance or conductivity measurements can be made to determine the number of particles and, therefore, target molecules that fill the gap. However, the sensitivity of the device can be markedly increased by exposing the active component of the device to a solution of Ag(I) and hydroquinone (photographic developing solution). The use of Au nanoparticles as promoters for Ag(I) reduction has been exploited in colorimetric detection schemes for DNA and proteins (*4*, *12*). Moreover, we and others have evaluated the electrical properties of DNA-modified nanoparticles, protein-modified nanoparticles, aggregates, and structures formed from Ag reduction on individual particles (*13*–*15*), and those data suggest that the system described in Fig. 1A should be viable, provided that enough particles can fill the gaps and give a measurable electrical signal.

Such a strategy can be extended to arrays (*16*), where each component of the array is an

Department of Chemistry and Institute for Nanotechnology, Northwestern University, Evanston, IL 60208, USA.

*Present address: Department of Chemistry, University of Minnesota, Minneapolis, MN 55455, USA.
†To whom correspondence should be addressed. E-mail: camirkin@chem.northwestern.edu

electrode pair with a different oligonucleotide capture strand in the electrode gap. We describe the performance of one such array, which consists of four elements designed to evaluate the selectivity of the system outlined in Fig. 1A. We also describe an unusual salt dependence on the melting properties of the hybridized particles that can be used to eliminate the need for a thermal-stringency wash to differentiate binding events involving mismatched strands from ones based on perfectly complementary recognition elements.

In a typical experiment, microelectrodes (60-nm Au on 5-nm Ti) with 20-μm gaps were prepared by standard photolithography on a Si wafer with a 1-μm coating of SiO_2 (Fig. 1C). The exposed SiO_2 of the entire chip was modified with succinimidyl 4-(malemidophenyl)-butyrate (SMPB; Sigma Chemical, St. Louis, MO) by using reported methods (*4*, *17*). Capture oligonucleotide strands were immobilized onto the activated surface by spotting 0.3 M NaCl, 10 mM phosphate buffer (pH 7) solutions [0.3 M phosphate-buffered saline (PBS)] of the appropriate alkylthiol-modified oligonucleotide (1 mM) in the electrode gaps by manual pipetting. All of the oligonucleotides used in this study were prepared by automated solid-phase syntheses (*3*, *18*). The DNA chip arrays were designed to evaluate the discrimination of the complementary pair, A:T (X = A), from the three single-base mismatches, T:T (X = T), C:T (X = C), or G:T (X = G) in a synthetic 27-base oligonucleotide target (based on the anthrax lethal factor sequence) (*19*). After spotting capture oligonucleotides in the electrode gaps, the chip was stored in a humidity chamber for 24 hours to allow the coupling reaction between the SMPB and alkylthiol-capped DNA to take place. The chip was then washed with water and immersed in 2% hexanethiol in ethanol for 2 hours to passivate the chip, including the Au electrodes. Finally, the DNA-functionalized chip was washed with ethanol and water and then dried under a stream of N_2.

To evaluate the detection capabilities of the array, we treated it with 0.3 M PBS solution of target DNA (10 nM) for 4 hours and rinsed it with 0.3 M PBS solution. It was then treated with a 0.3 M PBS solution of nanoparticle probes (2 nM, oligonucleotide-modified 13-nm diameter particles) (*3*) for 2 hours. The DNA chip was rinsed with 0.3 M $NaNO_3$ in 10 mM phosphate buffer (pH 7) to remove chloride ions and then treated with a silver enhancer solution (Sigma), which is composed of $AgNO_3$ and hydroquinone. The silver enhancer solution was replaced every 2 or 3 min to avoid the formation of silver particulate in solution. After each treatment of the chip with the silver enhancer solution, the chip was rinsed with water, then dried with N_2, and the resistance values across the electrode gaps were measured with a Fluke 189 multimeter (Fluke, Everett, WA). After a 3-min treatment with silver enhancer solution, the gaps with the four different oligonucleotide capture strands exhibit resistances greater than the limit of the multimeter (200 megohm) (Fig. 2A).

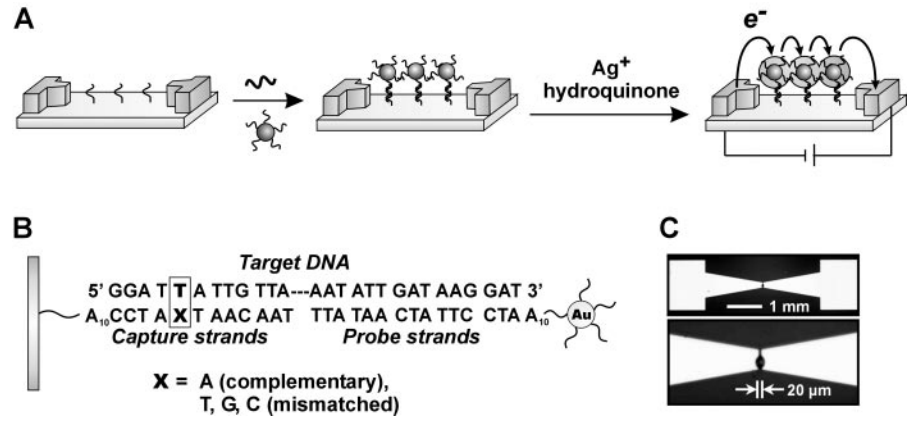

Fig. 1. (**A**) Scheme showing concept behind electrical detection of DNA. (**B**) Sequences of capture, target, and probe DNA strands. (**C**) Optical microscope images of the electrodes used in a typical detection experiment. The spot in the electrode gap in the high-magnification image is food dye spotted by a robotic arrayer (GMS 417 Microarrayer, Genetic Microsystems, Woburn, MA).

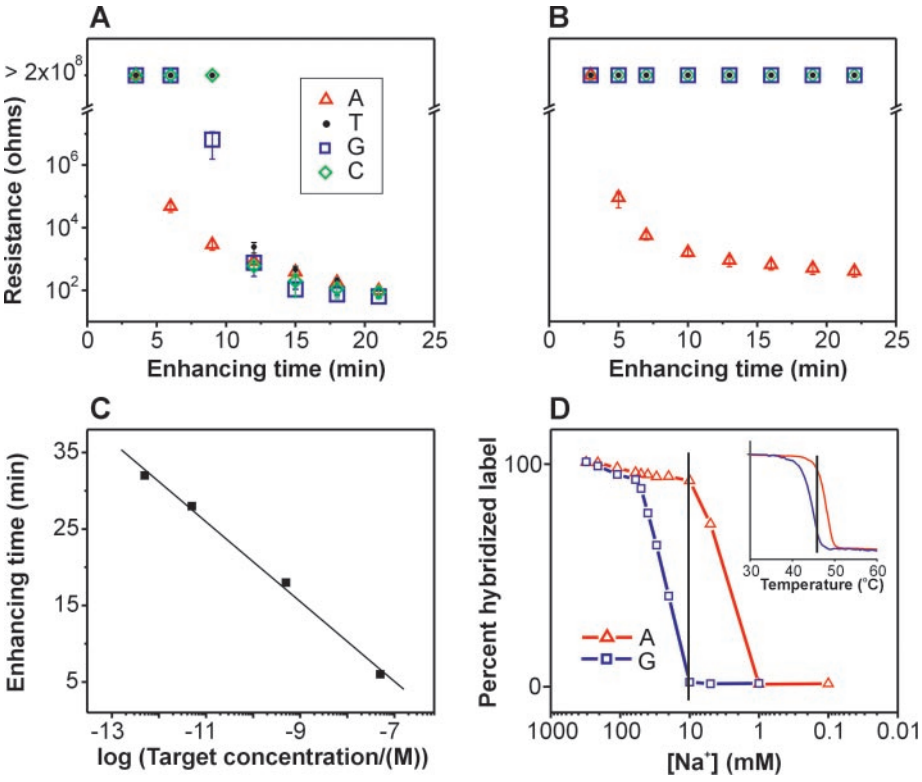

Fig. 2. Resistance of the electrode arrays measured as a function of increasing silver enhancing time (**A**) without and (**B**) with washing with 0.01 M PBS at room temperature before silver enhancing. (**C**) A graph of the silver enhancing time required to reach a resistance value of 100 kilohm as a function of target concentration showing that target can be detected in the 50 nM to 500 fM concentration range by adjusting silver enhancing time. Target DNA and nanoparticle probes were cohybridized to capture strand DNA in 0.6 M PBS for 6 hours in all quantification experiments; this procedure leads to slightly greater sensitivity than the aforementioned protocol. (**D**) DNA duplex denaturation curve as a function of $[Na^+]$ for the perfectly complementary oligonucleotide (X = A) and the strand with a wobble mismatch (X = G). For these experiments, the inside walls of glass cuvettes (Fisher Scientific, Pittsburgh, PA) were functionalized with the appropriate capture-strand oligonucleotide and then treated with 0.3 M PBS solution of target DNA (10 nM) for 10 hours followed by nanoparticle probes (2 nM) for 5 hours. The extinction at 520 nm (1:1 correlation with "% hybridized label") was monitored after washing the cuvettes with a series of buffer solutions containing different NaCl concentrations (*20*). (**Inset**) Thermal-denaturation curves for the perfectly matched DNA (X = A) and the one with a wobble mismatch (X = G).

In the absence of a stringency wash, the gap resistances decrease with increasing exposure to the silver enhancer solution for all complementary and noncomplementary strands (Fig. 2A). In a separate experiment, field emission scanning electron microscope (FE-SEM) images of an indium tin oxide (ITO) surface, treated in a manner identical to treatment of the electrode gaps, before and after silver deposition show that silver deposition increases with increasing exposure to the silver enhancer solution (Fig. 3, A to D). Interestingly, the particles all exhibit different growth rates. Indeed, even after 9 min of exposure to the enhancer solution, some particles remain unaffected in terms of size and shape. Thus, the nanoparticles initiate the silver deposition, but deposited silver further catalyzes the silver reduction, which is ultimately responsible for closing the circuit, rather than a process that results in uniform particle growth with eventual electrical shorting of those particles (*20*). The particles are complex materials and when considered on an individual basis, must have slightly different levels of oligonucleotide functionalization and, therefore, different activities with respect to their ability to promote the reduction of Ag^+ to Ag by hydroquinone. In the absence of target DNA, there was no detectable signal even after 40 min of silver enhancing. Using this method, we have detected target in the 50 nM to 500 fM concentration range without appreciable effort to optimize the system for sensitivity (Fig. 2C). The detection limit of a conventional fluorescence-based system that utilizes a confocal microscope, these oligonucleotide strands, and a Cy3-modified probe is ~ 5 pM (*4*).

A conventional way of increasing target selectivity is to wash a DNA chip array with a buffer solution at a temperature that results in the dehybridization of DNA duplexes formed from noncomplementary strands (*1*). We have shown previously that other nanoparticle-based DNA detection methods exhibit unusually high specificity because of the sharp melting transitions associated with duplex structures formed from oligonucleotide-modified nanoparticle probes and complementary oligonucleotides (*4*). Therefore, for the system reported here, one might expect to see a difference in resistance between the gaps modified with the perfectly complementary capture strand as compared with the gaps modified with the noncomplementary strands, when washed with a stringency solution at the appropriate temperature. Indeed, when the chip was washed with 0.3 M PBS at 50°C before treatment with the silver enhancer solution, the resistance for the gaps with the complementary capture strand decreased to 500 ohms with Ag enhancing time over a 3- to 20-min range, but all three of the gaps with the single-base mismatches showed resistances greater than 200 megohm, even after 20 min of enhancing time (*20*). In other words, a complementary strand in this experiment provides a signal that is at least 10^5 times greater than that of the noncomplementary strands. This selectivity is impressive, especially when one compares this value to the selectivity ratio observed in the comparable fluorescence-based approach (2.6:1) and even to that in the previously reported scanometric approach (11:1) (*4*).

We have found that oligonucleotide-modified nanoparticles exhibit unusually sharp denaturation properties over salt concentration gradients (Fig. 2D). Indeed, by examining the extinction at 520 nm of two glass cuvettes functionalized with the complementary capture strand–target–probe complex and the capture strand with G-T mismatch–target–probe complex, respectively, as a function of solution Na^+ concentration, one can easily differentiate the mismatched oligonucleotides from the complementary target. Importantly, one obtains better differentiation of the two strands using changes in salt concentration as opposed to changes in temperature (Fig. 2D, inset). Therefore, the nanoparticle probes on mismatched DNA can be selectively dehybridized by washing the chip with a buffer solution of the proper cation concentration. After a stringency wash of the chip with 0.01 M PBS at room temperature, the resistance of the gap with the perfectly complementary DNA (X = A) substantially decreases with silver deposition, whereas all three gaps functionalized with the mismatched strands (X = T, G, or C) remain insulating, even after 20 min of enhancing time (Fig. 2B). In control experiments, when the DNA chip was washed with water in order to denature all of the duplex strands, there was no detectable signal for all four DNA strands after 40 min of silver enhancing. The use of salt concentration as a stringency tool may eliminate the need for thermocyclers in array-based detection systems and also opens up opportunities for using probes that suffer from instability at elevated temperatures. Finally, because this system is based on conventional microelectrodes, it is positioned for massive multiplexing through the use of larger arrays of electrode pairs than the four used in the proof-of-concept experiments reported here.

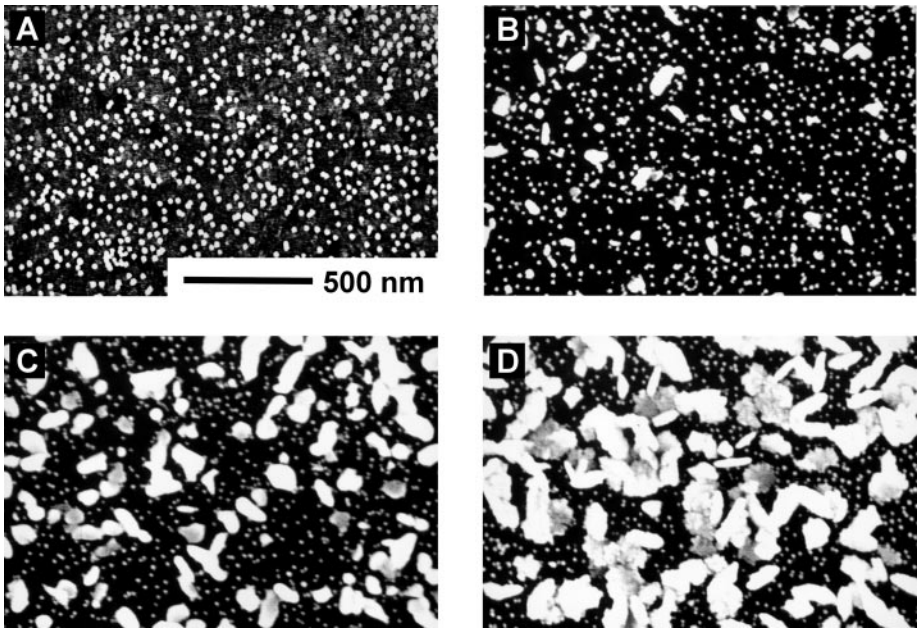

Fig. 3. FE-SEM images of the nanoparticle probes on an ITO-coated glass surface (**A**) before silver deposition, (**B**) after a 3-min treatment with the enhancer solution, (**C**) after a 6-min treatment with the enhancer solution, and (**D**) after a 9-min treatment with silver enhancer solution. ITO-coated glass substrates (Delta Technologies, Stillwater, MN) were modified with complementary capture DNA strands, and the target DNA and oligonucleotide-modified nanoparticles were assembled on the substrates following the same procedure used for DNA detection (*21*).

References and Notes

1. G. H. Keller, M. M. Manak, *DNA Probes* (Stocktonton, NY, 1989).
2. R. Elghanian, J. J. Storhoff, R. C. Mucic, R. L. Letsinger, C. A. Mirkin, *Science* **277**, 1078 (1997).
3. J. J. Storhoff, R. Elghanian, R. C. Mucic, C. A. Mirkin, R. L. Letsinger, *J. Am. Chem. Soc.* **120**, 1959 (1998).
4. T. A. Taton, C. A. Mirkin, R. L. Letsinger, *Science* **289**, 1757 (2000).
5. T. A. Taton, G. Lu, C. A. Mirkin, *J. Am. Chem. Soc.* **123**, 5164 (2001).
6. M. E. Napier *et al.*, *Bioconjugate Chem.* **8**, 906 (1997).
7. S. O. Kelly, E. M. Boon, J. K. Barton, N. M. Jackson, M. G. Hill, *Nucleic Acids Res.* **27**, 4830 (1999).
8. C. J. Yu *et al.*, *J. Am. Chem. Soc.* **123**, 11155 (2001).
9. L. He *et al.*, *J. Am. Chem. Soc.* **122**, 9071 (2000).
10. W. C. W. Chan, S. Nie, *Science* **281**, 2016 (1998).
11. S. R. Nicewarner-Pena *et al.*, *Science* **294**, 137 (2001).

12. C. M. Niemeyer, B. Ceyhan, *Angew. Chem. Int. Ed.* **40**, 3685 (2001).
13. O. D. Velev, E. W. Kaler, *Langmuir* **15**, 3693 (1999).
14. S.-J. Park *et al.*, *Angew. Chem. Int. Ed.* **39**, 3845 (2000).
15. R. Moller, A. Csaki, J. M. Kohler, W. Fritzsche, *Langmuir* **17**, 5426 (2001).
16. S. P. A. Fodor, *Science* **277**, 393 (1997).
17. L. A. Chrisey, G. U. Lee, C. E. O'Ferrall, *Nucleic Acids Res.* **24**, 3031 (1996).
18. F. Eckstein, *Oligonucleotides and Analogues* (Oxford Univ. Press, New York, 1991).
19. S. Ikuta, K. Takagi, R. B. Wallace, K. Itakura, *Nucleic Acids Res.* **15**, 797 (1987).
20. Supplementary data are available on *Science* Online at www.sciencemag.org/cgi/content/full/295/5559/1503/DC1.
21. The nanoparticle coverage on the ITO surface does not necessarily correspond exactly with the coverage on the SiO_2 surface. However, the SEM images provide information about the silver-deposition process on an oxide surface modified with oligonucleotide-functionalized nanoparticles rather than a correlation between the amount of deposited silver and resistance values in Fig. 2.
22. C.A.M. acknowledges the Air Force Office of Scientific Research (DURINT) and the Defense Advanced Research Projects Agency for support of this research.

10 October 2001; accepted 17 January 2002

Efficient Near-Infrared Polymer Nanocrystal Light-Emitting Diodes

Nir Tessler,[1]* Vlad Medvedev,[1] Miri Kazes,[2] ShiHai Kan,[2] Uri Banin[2]*

Conjugated polymers and indium arsenide–based nanocrystals were used to create near-infrared plastic light-emitting diodes. Emission was tunable from 1 to 1.3 micrometers—a range that effectively covers the short-wavelength telecommunications band—by means of the quantum confinement effects in the nanocrystals. The external efficiency value (photons out divided by electrons in) is ~0.5% (that is, >1% internal) and is mainly limited by device architecture. The near-infrared emission did not overlap the charge-induced absorption bands of the polymer.

For certain device applications, semiconducting polymers can replace inorganic semiconductors at lower cost because they are more easily processed. Examples include the development of organic light-emitting diodes (OLEDs) for full-color screen applications, and the development of field-effect transistors for smart circuit applications (*1, 2*). The extension of OLEDs into the technologically important near-infrared (NIR) spectral range used in telecommunications is more difficult because organic molecules usually display optical activity only at wavelengths shorter than 1 μm.

Attempts have been made to extend organic-based light emission beyond 1 μm by using lanthanide complexes in which rare-earth atoms are incorporated into the molecules (*3–5*). Emission efficiency is generally low because of near-field deactivation by the host associated with coupling of the optically excited state to the vibrations of the organic molecule or polymer (*6*), the best reported internal efficiency value being 0.01% (*7*). Furthermore, the 1.5-μm band is effectively covered by the mature technology of erbium-doped fiber amplifiers (*8*), whereas similar devices for the 1.3-μm band are still being developed. Here we report the production of OLEDs, based on a combination of semiconducting polymers and NIR optically active semiconductor nanocrystals (NCs) (*9*), that cover the short-wavelength telecommunications band with internal efficiency values of >1%.

The incorporation of NCs with a semiconducting polymer in visible-range OLEDs (*10–13*) and photovoltaics (*14*) has been reported. We used a core-shell approach to produce NCs with strong emission in the NIR and increased photostability (*15, 16*). Optimized core-shell NC structures can shield the electron-hole pair that is localized to the core from the host deactivation paths while still allowing this active region to absorb energy from the host, either through charge transfer or through neutral-excitation energy transfer (as in the case of Förster or Dexter transfer mechanisms) (*17*). In combination with commercially available polymers (*18*), we fabricated LEDs with external efficiencies up to 0.5% [corresponding to 1.5 to 3% internal efficiency (*19, 20*)] where the emission center can be tuned up to 1.3 μm and the emission tail extends beyond 1.4 μm. The emission is taken out of the charge-induced absorption bands of the polymer (centered around ~800 nm), thus overcoming what is considered to be the main obstacle for achieving electrically pumped lasers in amorphous organic materials (*21*).

Core-shell InAs-ZnSe NCs with an average core radius of 2.4 nm and ZnSe shell with nominal thickness of 1.5 monolayers (Fig. 1A) with strong emission in the 1.3-μm range were prepared in a two-step synthesis, as reported previously (*15, 16*). Films of conjugated polymers—either poly[2-methoxy-5-(2-ethylhexyloxy)-1,4-phenylenevinylene] (MEH-PPV) or poly[(9,9-dihexylfluorenyl-2,7-diyl)-co-(1,4-{benzo-[2,1′,3]thiadiazole})] (F6BT) (Fig. 1) (*18, 22*)—and NCs were made by first creating separate NC and polymer solutions in toluene. Appropriate volumes were mixed to create the required NC/polymer volume ratio. Finally, the optical absorption of the composite film was measured and used as a final monitoring step. Optically homogeneous films were spin-cast from solution to ~100 nm thickness onto a suitable substrate (*23*). Typical absorption spectra of such films are shown in Fig. 1B. The absorption is essentially a combination of the two species. Above 800 nm, the absorption is due to quantum-confined transitions of the NCs, and below 600 nm, the host conjugated polymer contributes considerably,

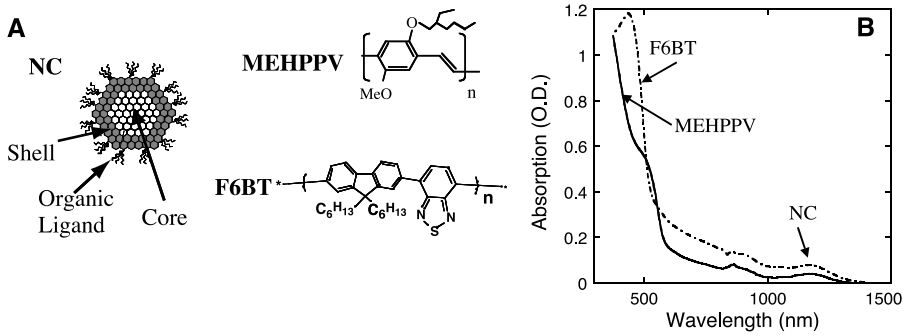

Fig. 1. (**A**) Structural description of the nanocrystal (NC) and of the polymers MEH-PPV and F6BT. (**B**) Optical absorption spectra of MEH-PPV–NC (solid line) and F6BT-NC (dashed line) films with approximately equal volume ratio.

[1]Electrical Engineering Department, Microelectronic Center, and Communications and Information Technologies Center, Technion–Israel Institute of Technology, Haifa 32000, Israel. [2]Institute of Chemistry and the Center for Nanoscience and Nanotechnology, Hebrew University, Jerusalem 91904, Israel.

*To whom correspondence should be addressed. E-mail: nir@ee.technion.ac.il, banin@chem.ch.huji.ac.il